

LETTER TO THE EDITOR

More sulphur in TMC-1: Discovery of the NC₃S and HC₃S radicals with the QUIJOTE line survey[★]

J. Cernicharo¹, C. Cabezas¹, M. Agúndez¹, R. Fuentetaja¹, B. Tercero^{2,3}, N. Marcelino^{2,3}, and P. de Vicente³

¹ Dept. de Astrofísica Molecular, Instituto de Física Fundamental (IFF-CSIC), C/ Serrano 121, 28006 Madrid, Spain.
e-mail: jose.cernicharo@csic.es

² Observatorio Astronómico Nacional (OAN, IGN), C/ Alfonso XII, 3, 28014, Madrid, Spain.

³ Observatorio de Yebes (IGN). Cerro de la Palera s/n, 19141 Yebes, Guadalajara, Spain

Received: 26/06/2024; accepted: 05/07/2024

ABSTRACT

We present the detection of the free radicals NC₃S and HC₃S towards TMC-1 with the QUIJOTE line survey. The derived column densities are $(1.4 \pm 0.2) \times 10^{11}$ for NC₃S and $(1.5 \pm 0.2) \times 10^{11}$ for HC₃S. We searched for NCCS, but only three transitions are within the domain of our QUIJOTE line survey and the observed lines are marginally detected at the 3σ level, providing an upper limit to its column density of $\leq 6 \times 10^{10}$ cm⁻². We also unsuccessfully searched for longer species of the NC_nS ($n \geq 4$) and HC_nS ($n \geq 5$) families in our TMC-1 data. A chemical model based on a reduced set of reactions involving HC₃S and NC₃S predicts abundances that are 10-100 times below the observed values. These calculations indicate that the most efficient reactions of formation of HC₃S and NC₃S in the model are S + C₃H₂ and N + HC₃S, respectively, while both radicals are very efficiently destroyed through reactions with neutral atoms.

Key words. molecular data — line: identification — ISM: molecules — ISM: individual (TMC-1) — astrochemistry

1. Introduction

A significant number of S-bearing species have been detected in the starless core TMC-1. In particular, the species CS, CCS, and CCCS are among the most abundant molecules in cold dark clouds (Saito et al., 1987; Yamamoto et al., 1987; Kaifu et al., 1987) and in the circumstellar envelopes of carbon-rich evolved stars (Cernicharo et al., 1987a). The abundance and variety of sulphur-bearing species detected to date in cold clouds is hampered, to a large extent, by the significant depletion of sulphur in the cloud (Vidal et al., 2017; Fuente et al., 2019; Navarro-Almaida et al., 2020; Fuente et al., 2023, and references therein) and by the lack of sensitive line surveys that allow the detection of low-abundance, or high-abundance but low-dipole moment, S-bearing molecules.

In the last four years, our knowledge of the chemical composition of TMC-1 regarding sulphur has experienced an enormous advancement with the discovery of 14 new sulphur-bearing molecules thanks to the ultra-sensitive QUIJOTE¹ line survey (Cernicharo et al., 2021a). Neutral species such as C₄S, C₅S (previously detected only towards evolved stars), HCCS, H₂CCS, H₂CCCS, NCS, HSO, HCSCN, HCSCCH, HC₄S, HCNS, and NCCHCS have been detected with QUIJOTE (Cernicharo et al., 2021b,c; Fuentetaja et al., 2022; Marcelino et al., 2023; Cernicharo et al., 2024a; Cabezas et al., 2024). In addition,

cations such as HCCS⁺ (Cabezas et al., 2022) and HC₃S⁺ (Cernicharo et al., 2021d) have also been found in this cloud. Chemical models are being continuously improved and refined to shed light on the formation and destruction pathways of all these newly detected species.

The continuous sensitivity increase of the QUIJOTE line survey makes it well suited to detect additional heavier S-bearing species. In this context we present in this Letter the discovery, for the first time in space, of the radicals HC₃S and NC₃S. Only upper limits have been obtained for the column densities of longer members of the HC_nS and NC_nS families. The formation and destruction pathways of HC₃S and NC₃S are analysed with state-of-the-art chemical models. With the detection of HC₃S and NC₃S, QUIJOTE has provided the identification of 16 new S-bearing molecules in space.

2. Observations

The observational data used in this work are from QUIJOTE (Cernicharo et al., 2021a), a spectral line survey of TMC-1 in the Q band carried out with the Yebes 40m telescope at the position $\alpha_{J2000} = 4^{\text{h}}41^{\text{m}}41.9^{\text{s}}$ and $\delta_{J2000} = +25^{\circ}41'27.0''$, which corresponds to the cyanopolyne peak in TMC-1. The receiver was built as part of the Nanocosmos project² and consists of two cold high-electron mobility transistor amplifiers covering the 31.0-50.3 GHz band with horizontal and vertical polarizations. Receiver temperatures vary between 16 K at 32 GHz and 30 K at 50 GHz. The back ends are $2 \times 8 \times 2.5$ GHz fast Fourier transform spectrometers with a spectral resolution of 38 kHz, providing the whole coverage of the Q band in both polariza-

[★] Based on observations with the Yebes 40m telescope (projects 19A003, 20A014, 20D023, 21A011, 21D005, and 23A024). The 40 m radio telescope at Yebes Observatory is operated by the Spanish Geographic Institute (IGN; Ministerio de Transportes y Movilidad Sostenible).

¹ Q-band Ultrasensitive Inspection Journey to the Obscure TMC-1 Environment

² <https://nanocosmos.iff.csic.es/>

tions. A detailed description of the system is given by Tercero et al. (2021), and details on the QUIJOTE line survey observations have previously been provided (Cernicharo et al., 2021a, 2023a,b, 2024a,b). The frequency switching method was used for all observations. The data analysis procedure has been described by Cernicharo et al. (2022). The total observing time on source is 1202 hours, and the measured sensitivity varies between 0.08 mK at 32 GHz and 0.2 mK at 49.5 GHz.

The main beam efficiency can be given across the Q band as $\eta_{\text{eff}} = 0.797 \exp[-(\nu(\text{GHz})/71.1)^2]$. The forward telescope efficiency is 0.95, and the beam size at half power intensity is $54.4''$ and $36.4''$ at 32.4 and 48.4 GHz, respectively. The absolute intensity calibration uncertainty is 10%, although the relative calibration between lines within the QUIJOTE survey is certainly better because all of them are observed simultaneously and have the same calibration uncertainties and systematic effects. The data were analysed with the GILDAS package³.

3. Results

Line identification in this work was performed using the MADEX code (Cernicharo, 2012), in addition to the CDMS and JPL catalogues (Müller et al., 2005; Pickett et al., 1998). The intensity scale utilized in this study is the antenna temperature (T_A^*). Consequently, the telescope parameters and source properties were used when modelling the emission of the different species to produce synthetic spectra on this temperature scale. In this work we assumed a velocity for the source relative to the local standard of rest of 5.83 km s^{-1} (Cernicharo et al., 2020). The source was assumed to be circular with a uniform brightness temperature and a radius of $40''$ (Fossé et al., 2001). Line parameters for all observed transitions with the Yebes 40m radio telescope were derived by fitting a Gaussian line profile to them using the GILDAS package. A velocity range of $\pm 20 \text{ km s}^{-1}$ around each feature was considered for the fit after a polynomial baseline was removed. Negative features produced in the folding of the frequency switching data were blanked before baseline removal. The observed line intensities were modelled using a local thermodynamical equilibrium hypothesis. The laboratory data used in this work are discussed in the following sections. We first discuss NC_3S because its detection motivated the search for NCCS and other longer NC_nS chains.

3.1. Discovery of NC_3S

We have found a series of six harmonically related lines with half-integer quantum numbers from $J=23/2-21/2$ to $J=33/2-31/2$. The lines are shown in Fig. 1. The two first lines clearly show hyperfine structure, which suggests the presence of a nitrogen atom in the molecule. The other lines are also broader with respect to the standard lines from other species ($\Delta v = 0.6-0.7 \text{ km s}^{-1}$). We were able to fit the frequency centroids (see Table 1) with the standard relation for the frequencies of a linear molecule, finding an effective rotational constant, B_{eff} , of $1438.9761 \pm 0.0003 \text{ MHz}$ and an effective distortion constant, D_{eff} , of $47.6 \pm 0.6 \text{ Hz}$. The standard deviation of the fit is 4.1 kHz. We verified that the lines cannot be produced by a species with a rotational constant half of the derived one (all lines with even J s would be missing in that case). The half-integer quantum numbers indicate that the carrier is a radical.

The lines do not appear in any of the line catalogues available to us. The recent discovery of HC_5N^+ with a rotational constant

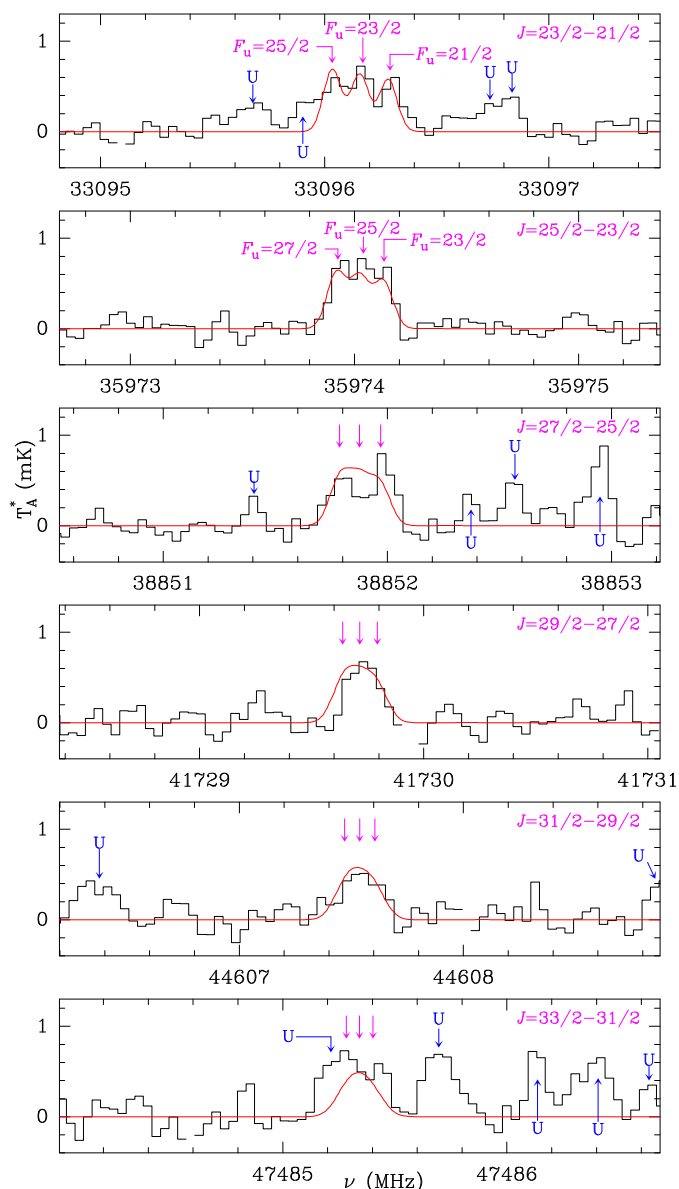


Fig. 1. Observed transitions of NC_3S . Quantum numbers are indicated at the top right of each panel. The abscissa corresponds to the rest frequency. The ordinate is the antenna temperature, corrected for atmospheric and telescope losses, in millikelvins. Blank channels correspond to negative features produced when folding the frequency-switched data. The purple vertical arrows indicate the position of the three strongest hyperfine components for each transition, corresponding to $F_u = J_u + 1$, J_u , and $J_u - 1$. The red line shows the modelled spectra for NC_3S with the physical parameters given in Sect. 3.1.

of 1336.6 MHz (Cernicharo et al., 2024b) pointed us towards the possibility of an isomer of this molecule. Accurate ab initio calculations, however, permitted us to discard all of them. A species recently detected in TMC-1 is HC_4S (Fuentetaja et al., 2022), which has a rotational constant of 1435.3 MHz and a $^2\Pi$ inverted ground electronic state (Hirahara et al., 1994). Hence, the carrier should be a molecule similar to HC_4S but containing a nitrogen atom. Taking into account that NCS has already been detected in TMC-1 (Cernicharo et al., 2021b), we conclude that NC_3S is a solid candidate to be the carrier of the observed lines. This species was not included in the MADEX code, nor in the CDMS or JPL catalogues. However, a quick search in the literature indicates that the molecule has been studied in the lab-

³ <http://www.iram.fr/IRAMFR/GILDAS>

Table 1. Estimated line parameters for the observed lines of NC₃S.

$J_u - J_l$	$F_u - F_l$	ν_{obs}^a (MHz)	obs.-calc. (kHz)	$\int T_A^* dv^b$ (mK km s ⁻¹)	Δv^c	T_A^{*d} (mK)	Notes
23/2-21/2		33096.164±0.020	2.6	1.79±0.11	3.02	0.61±0.09	A
23/2-21/2	25/2-23/2	33096.047±0.020	13.0	0.53±0.05	0.70 ^e	0.71±0.09	
23/2-21/2	23/2-21/2	33096.168±0.020	-11.0	0.61±0.05	0.70 ^e	0.83±0.09	
23/2-21/2	21/2-19/2	33096.303±0.020	20.0	0.50±0.05	0.70 ^e	0.66±0.09	
25/2-23/2		35974.029±0.020	-2.3	1.73±0.11	2.10	0.78±0.08	
25/2-23/2	27/2-25/2	35973.943±0.020	23.0	0.74±0.14	0.90±0.22	0.77±0.08	
25/2-23/2	25/2-23/2	35974.048±0.020	25.0	0.46±0.18	0.61±0.25	0.76±0.08	
25/2-23/2	23/2-21/2	35974.138±0.020	11.0	0.48±0.12	0.62±0.09	0.72±0.08	
27/2-25/2		38851.890±0.020	3.0	1.27±0.11	2.20	0.54±0.11	
29/2-27/2		41729.725±0.020	-2.2	0.82±0.10	1.20	0.70±0.12	
31/2-29/2		44607.546±0.020	-4.9	0.76±0.08	1.39	0.51±0.11	
33/2-31/2		47485.361±0.020	4.1	0.89±0.18	1.30	0.69±0.15	A

Notes. ^(a) Observed frequency adopting a v_{LSR} of 5.83 km s⁻¹ for the source (Cernicharo et al., 2020). If F is not given, then the value refers to the frequency centroid and the calculated frequency is obtained from B_{eff} and D_{eff} . For lines with resolved hyperfine structure, the calculated frequencies have been obtained from a fit to the laboratory data from McCarthy et al. (2003). ^(b) Integrated line intensity in mK km s⁻¹. ^(c) Equivalent line width (in km s⁻¹). ^(d) Antenna temperature in millikelvins. ^(e) Line width has been fixed. ^(A) Partially blended with an identified feature.

oratory by McCarthy et al. (2003), together with other longer members of the NC_{*n*}S family.

NC₃S has an inverted ²Π ground electronic state, and the transitions observed in the laboratory by McCarthy et al. (2003) cover from $J=5/2-3/2$ up to $J=17/2-15/2$, which corresponds to frequencies up to 24.46 GHz. These data were fitted using SPFIT (Pickett et al., 1991), and the molecule was implemented in the MADEX code to produce predictions in the frequency domain of QUIJOTE. The spin-orbit constant was fixed to the value given by McCarthy et al. (2003), $A_{SO}=-9.8209$ THz. With such a high value for the spin-orbit constant, the energy levels of the ²Π_{1/2} ladder are above 470 K, and hence, no lines from this state are expected in TMC-1, where the kinetic temperature is 9 K (Agúndez et al., 2023). The derived rotational constant is $B_0=1439.18582±0.00008$ MHz, from which an effective rotational constant for the ²Π_{3/2} ladder can be derived from the relation $B_{eff}=B_0(1+B_0/A_{SO})$. Using the molecular constants derived by McCarthy et al. (2003), we derive $B_{eff}(^2\Pi_{3/2})=1438.97492±0.00008$ MHz, which is nearly identical to that derived for our series of lines in TMC-1 (a difference of 1.2 kHz). The distortion constant of NC₃S derived from the laboratory data is 45.8±0.8 Hz, also in excellent agreement with that derived for our series of lines. Hence, we conclude that the carrier of our lines is, without any doubt, NC₃S.

The lines observed in the laboratory for this species exhibit a prominent hyperfine structure introduced by the nitrogen nucleus. However, no Λ-doubling splitting was found. As an example, the three strongest components of the $J=17/2-15/2$ transition at 24.6 GHz span 0.5 MHz. The frequency predictions indicate that the $J=23/2-21/2$ and $25/2-23/2$ lines observed in TMC-1 will show a considerable splitting, as observed in our lines (see Fig. 1). All the other transitions within the frequency range of our data are predicted to have a significant line broadening. We merged the astronomical frequencies with the laboratory values to try to improve the rotational constants of NC₃S. However, such an improvement was marginal as the derived parameters are nearly the same as those of McCarthy et al. (2003).

To derive the column density of NC₃S, we adopted a dipole moment of 3.0 D (McCarthy et al., 2003). We fitted the observed line profiles and intensities assuming a source of uniform brightness temperature. We obtain $T_{rot}=5.5±0.5$ K and a column den-

sity of $(1.4±0.2)×10^{11}$ cm⁻². The source diameter that best fits the data is 70". The observed line profiles are nicely reproduced by the modelled synthetic spectra shown in red in Fig. 1.

3.2. Search for NCCS and longer NC_{*n*}S chains

Since NCS and NC₃S are detected (Cernicharo et al., 2021b, and this work), it was worthwhile searching for NCCS in our data. Similarly to NC₃S, the NCCS species was not included in the MADEX code, nor in the CDMS or JPL catalogues. However, the bent radical NCCS (X^2A') was studied via Fourier-transform microwave spectroscopy by Nakajima et al. (2003) up to 22.6 GHz, corresponding to the $4_{04}-3_{03}$ transition. Only $K_a=0$ transitions were observed in the laboratory. The observed frequencies were fitted using the SPFIT code (Pickett et al., 1991) to produce predictions in the frequency domain of QUIJOTE. The A constant was fixed to 186.47 GHz; hence, the $K_a=1$ lines are ~9 K above the $K_a=0$ ones and will have a considerable frequency uncertainty. The first $K_a=1$ line in our data is the $6_{16}-5_{15}$ with an upper energy level at 14.4 K. For an expected rotational temperature of 5-6 K, as found for another three or four atoms species, the expected intensities of the $K_a=1$ lines will be a factor of five weaker than those of the $K_a=0$ ones. Three transitions with $K_a=0$ can be explored with our data ($N_{up}=6, 7, \text{ and } 8$). These lines show two fine components with $J=N+1/2$ and $J=N-1/2$, and an additional hyperfine splitting introduced by the nitrogen atom. The fine and hyperfine components of each rotational transition span 200 kHz. Unfortunately, some lines are blended, and the other lines are only detected at a marginal 3σ level. The dipole moment of NCCS has been calculated to be 2.49 D (McCarthy et al., 2003). Using this value, we derive a 3σ upper limit to the column density of this radical of $≤6×10^{10}$ cm⁻².

Laboratory data for NC₄S, NC₅S, NC₆S, and NC₇S are also available from the study of McCarthy et al. (2003). We implemented these molecules in MADEX and searched for them in our data. However, none of their lines were detected. The 3σ upper limits to their column densities are in the range $(8-10)×10^{10}$ cm⁻².

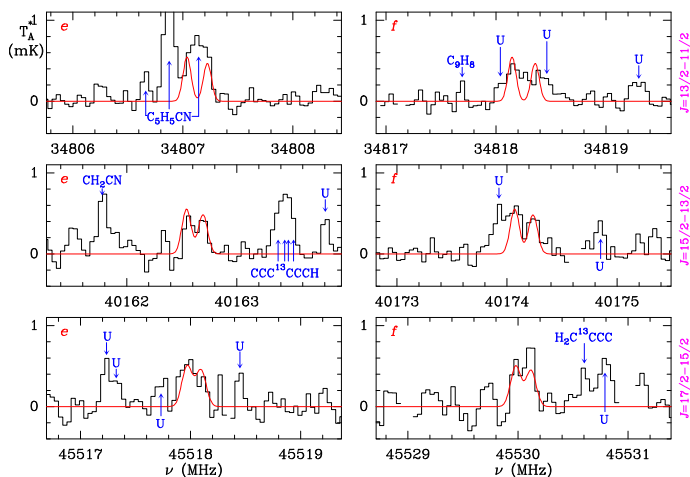


Fig. 2. Observed transitions of HC_3S . Quantum numbers are indicated at the right side of each row. The abscissa corresponds to the rest frequency. The ordinate is the antenna temperature, corrected for atmospheric and telescope losses, in millikelvins. Blank channels correspond to negative features produced when folding the frequency-switched data. The Λ -doubling components e and f for each J are shown in the left and right panels, respectively. In addition, the two hyperfine components of each e and f rotational transition are resolved in our data and appear clearly detected. They correspond to $F_u = J_u + 1/2$ and $J_u - 1/2$. The red line shows the modelled spectra for HC_3S with the physical parameters given in Sect. 3.3.

3.3. Discovery of HC_3S

HCCS and HC_4S have been detected in TMC-1 (Cernicharo et al., 2021b; Fuentetaja et al., 2022); hence, we could expect HC_3S to also be present in the cloud. Rotational spectroscopy for HC_3S is available from the studies of McCarthy et al. (1994) and Hirahara et al. (1994). The dipole moment was estimated to be 1.76 D through ab initio calculations (McCarthy et al., 1994). Frequency predictions for this species are available in the CDMS catalogue; hence, we implemented them into the MADEX code to obtain frequency predictions for the rotational transitions inside the frequency coverage of QUIJOTE. Three of these transitions – with $J_{\text{up}} = 13/2, 15/2,$ and $17/2$ – are in our data.

The lines of the ${}^2\Pi_{1/2}$ ladder of HC_3S exhibit Λ -doubling splitting that produces two components, e and f , for each rotational transition. In addition, each of these e and f components is further split into two hyperfine components due to the spin $1/2$ of the unpaired electron. Hence, the three rotational transitions of HC_3S that can be observed in our data will produce a total of 12 well-resolved features. Figure 2 shows the observed lines. Although the e component of the $J=13/2-11/2$ transition is partially blended with $\text{C}_5\text{H}_5\text{CN}$, the two hyperfine components can be seen and adjusted. All the other lines are well detected. However, due to the partial blending between the $F_u = J_u + 1/2$ and $F_u = J_u - 1/2$ hyperfine components, a fixed linewidth of 0.7 km s^{-1} was adopted for all the lines. We conclude that we have detected enough individual lines of HC_3S in TMC-1 to confidently claim its first detection in space. The derived line parameters are given in Table 2.

We adopted the same physical parameters for the cloud as for NC_3S and derive a rotational temperature of $6.0 \pm 0.5 \text{ K}$ and a column density of $(1.5 \pm 0.2) \times 10^{11} \text{ cm}^{-2}$, which is roughly a factor of two below the upper limit derived by Cernicharo et al. (2021b). The HCS and HCCS column densities have been derived to be $(5.5 \pm 0.5) \times 10^{12}$ and $(6.8 \pm 0.6) \times 10^{11} \text{ cm}^{-2}$, respectively (Cernicharo et al., 2021b). HC_4S was recently discovered

Table 2. Estimated line parameters for the observed lines of HC_3S .

Transition ^a (J_u, p, F_u)	ν_{cal} ^b (MHz)	$\int T_A^* dv$ ^c (mK km s ⁻¹)	v_{LSR} ^d (km s ⁻¹)	T_A^* ^e (mK)	Notes
13/2,e,7	34807.038	0.42±0.08	5.72±0.10	0.56±0.07	A
13/2,e,6	34807.223	0.49±0.07	5.86±0.07	0.66±0.07	A
13/2,f,7	34818.146	0.40±0.05	5.73±0.08	0.51±0.07	B
13/2,f,6	34818.356	0.40±0.05	5.57±0.10	0.37±0.07	B
15/2,e,8	40162.543	0.33±0.08	5.67±0.08	0.49±0.08	
15/2,e,7	40162.693	0.34±0.09	5.82±0.08	0.45±0.08	
15/2,f,8	40174.070	0.51±0.06	5.77±0.05	0.69±0.10	C
15/2,f,7	40174.236	0.40±0.06	5.79±0.06	0.53±0.10	
17/2,e,9	45517.969	0.27±0.06	5.88±0.14	0.36±0.13	
17/2,e,8	45518.095	0.47±0.06	5.89±0.09	0.63±0.13	
17/2,f,9	45529.980	0.33±0.10	5.83±0.09	0.60±0.13	
17/2,f,8	45530.118	0.56±0.11	5.90±0.07	0.80±0.13	

Notes. ^(a) Rotational upper quantum numbers. All transitions correspond to $\Delta J = \Delta F = +1$. ^(b) Predicted frequencies from a fit to the laboratory data (McCarthy et al., 1994; Hirahara et al., 1994). The uncertainty for all frequencies is 2 kHz. ^(c) Integrated line intensity in mK km s^{-1} . ^(d) Derived velocity with respect to the standard local of rest (LSR) in km s^{-1} . ^(e) Antenna temperature in millikelvins. ^(A) Partially blended with a line from $\text{C}_5\text{H}_5\text{CN}$. The line is between the two hyperfine components of this transition of HC_3S . ^(B) Partially blended with two unknown features. The derived line parameters are uncertain. ^(C) This line is partially contaminated by an unknown feature at a velocity of 6.9 km s^{-1} . The unknown and HC_3S features can be fitted reasonably well.

towards TMC-1 by Fuentetaja et al. (2022) with an estimated column density of $(9.5 \pm 0.8) \times 10^{10} \text{ cm}^{-2}$. Consequently, we derive the following abundance ratios: $\text{HCS}/\text{HCCS} = 8.1 \pm 1.6$, $\text{HCCS}/\text{HC}_3\text{S} = 4.5 \pm 1.0$, and $\text{HC}_3\text{S}/\text{HC}_4\text{S} = 1.6 \pm 0.3$. It seems, hence, that longer members of the HC_nS family could be present in significant abundances in TMC-1.

HC_5S was observed in the laboratory by Gordon et al. (2002). Frequency predictions for this species are included in the CDMS catalogue and have been used to implement the molecule in MADEX. Adopting an abundance ratio between HC_4S and HC_5S similar to that between HC_3S and HC_4S , we could expect a column density for HC_5S of $\sim 6 \times 10^{10} \text{ cm}^{-2}$. For a rotational temperature of 6 K, the expected line intensities for the $J=37/2-35/2$ transition at 32.4 GHz are $\sim 0.2 \text{ mK}$. These intensities are just the 3σ level of QUIJOTE, and, unfortunately, none of the lines of HC_5S have been detected. The same applies to longer members of the HC_nS family.

4. Discussion

The chemistry of sulphur-bearing molecules in cold dark clouds has recently been studied by Vidal et al. (2017), Vastel et al. (2018), and Laas & Caselli (2019) based on new chemical network developments. These studies reveal that the chemistry of sulphur in these cold clouds depends strongly on the degree of depletion of this element onto dust grains. Chemical networks are rather incomplete when dealing with S-bearing species. For example, of the first species detected in TMC-1 with QUIJOTE (NCS , HCCS , H_2CCS , H_2CCCS , C_4S , and C_5S), only C_4S was included in the chemical networks RATE12 (UMIST; McElroy et al., 2013) and kida.uva.2014 (KIDA; Wakelam et al., 2015). Vidal et al. (2017) made a significant effort to expand the number of reactions involving S-bearing species, including some of the species that were later detected with QUIJOTE. The latest chemical network release of the UMIST database (Millar et al., 2024) included many of the reactions first introduced by Vidal et al. (2017).

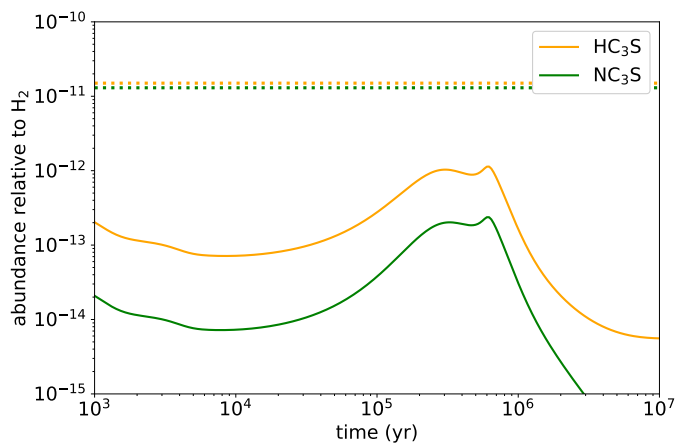


Fig. 3. Calculated fractional abundances of HC₃S and NC₃S as a function of time. Horizontal dotted lines correspond to the values observed in TMC-1 when adopting a column density of H₂ of 10²² cm⁻² (Cernicharo & Guélin, 1987).

To investigate the formation mechanism of HC₃S and NC₃S in TMC-1, we carried out chemical modelling calculations by adopting physical parameters of a standard cold dense cloud (Agúndez & Wakelam, 2013) and using the UMIST 2022 chemical network (Millar et al., 2024). The number of reactions involving our newly detected species is very limited. HC₃S appears as reactant in 16 reactions and as a product in only 10 reactions, and NC₃S was not included. According to our calculations, the main formation reaction of HC₃S is S + C₃H₂, followed by the dissociative recombination of HC₃SH⁺, and the reaction between C and H₂CCS. We included additional neutral–neutral reactions assuming that they occur through H atom elimination with a rate coefficient of 10⁻¹⁰ cm³ s⁻¹ (CH₂ + C₂S, CH + HCCS, SH + C₃H, and C₂H + HCS), but they are not as efficient as S + C₃H₂. In the model, HC₃S is mainly destroyed through reactions with neutral atoms (O, N, and C), which are assumed to occur fast according to Vidal et al. (2017). The resulting peak abundance calculated for HC₃S lies one order of magnitude below the observed one (see Fig. 3). It is unclear whether the chemical model is missing reactions of formation or if it is overestimating the destruction via reactions with neutral atoms.

The chemistry of NC₃S is completely unexplored. To shed some light on the possible formation mechanism of this radical, we included several neutral–neutral reactions that could lead to NC₃S, adopting a rate coefficient of 10⁻¹⁰ cm³ s⁻¹. These reactions are N + HC₃S, C₃N + SO, C₃N + S₂, C₃N + SH, and NH + C₃S. Based on the main destruction processes of NCS (which is included in the UMIST 2022 network), we assumed that NC₃S is mainly destroyed through reactions with O, H, and C atoms, and via reactions with abundant cations such as HCO⁺, H₃O⁺, and H₃⁺. The calculated abundance of NC₃S is shown in Fig. 3, which shows that the peak calculated abundance lies 50 times below the observed value. The main formation reaction of NC₃S is N + HC₃S. Since in the model HC₃S is the main precursor of NC₃S, the abundance of the latter closely follows that of the former (see Fig. 3).

Taking into account the reduced set of reactions involving HC₃S and NC₃S that are included in the chemical model and the large uncertainties in the reaction rate coefficients, the predictions of the chemical model regarding these two molecules should be viewed with caution, just as an order of magnitude estimate. A careful study of the main reactions that are identified

here to most influence these two molecules, namely S + C₃H₂ and N + HC₃S, together with the reactions of HC₃S and NC₃S with neutral atoms would provide a more accurate view of the underlying chemical processes responsible for the presence of these two peculiar S-bearing molecules in the cold dark cloud TMC-1.

Acknowledgements. We thank Ministerio de Ciencia e Innovación of Spain (MICIU) for funding support through projects PID2019-106110GB-I00, and PID2019-106235GB-I00. We also thank ERC for funding through grant ERC-2013-Syg-610256-NANOCOSMOS. We thank the Consejo Superior de Investigaciones Científicas (CSIC; Spain) for funding through project PIE 2022501097.

References

- Agúndez, M., Wakelam, V. 2013, *Chem. Rev.*, 113, 8710
- Agúndez, M., Marcelino, N., Tercero, B., et al. 2023, *A&A*, 677, A106
- Cabezas, C., Agúndez, M., Marcelino, N., et al. 2022, *A&A*, 657, L4
- Cabezas, C., Agúndez, M., Endo, Y. et al. 2024, *A&A*, 686, L3
- Cernicharo, J., Guélin, M., Hein, H. Kahane, C. 1987a, *A&A*, 181, L9
- Cernicharo, J. & Guélin, M. 1987b, *A&A*, 176, 299
- Cernicharo, J., 2012, in *ECLA 2011: Proc. of the European Conference on Laboratory Astrophysics*, EAS Publications Series, 2012, Ed.: C. Stehl, C. Joblin, & L. d’Hendecourt (Cambridge: Cambridge Univ. Press), 251; https://nanocosmos.iff.csic.es/?page_id=1619
- Cernicharo, J., Marcelino, N., Agúndez, M. et al. 2020, *A&A*, 642, L8
- Cernicharo, J., Agúndez, M., Kaiser, R.J., et al. 2021a, *A&A*, 652, L9
- Cernicharo, J., Cabezas, C., Agúndez, M., et al. 2021b *A&A*, 648, L3
- Cernicharo, J., Cabezas, C., Endo, Y., et al. 2021c, *A&A*, 650, L14
- Cernicharo, J., Cabezas, C., Endo, Y. et al. 2021d, *A&A*, 646, L3
- Cernicharo, J., Fuentetaja, R., Agúndez, M. et al. 2022, *A&A*, 663, L9
- Cernicharo, J., Pardo, J.R., Cabezas, C. et al. 2023a, *A&A*, 670, L19
- Cernicharo, J., Fuentetaja, R., Agúndez, M. et al. 2023b, *A&A*, 680, L4
- Cernicharo, J., Agúndez, M., Cabezas, C., et al. 2024a, *A&A*, 682, L4
- Cernicharo, J., Cabezas, C., Agúndez, M., et al. 2024b, *A&A*, 686, L15
- Fossé, D., Cernicharo, J., Gerin, M., Cox, P. 2001, *ApJ*, 552, 168
- Fuente, A., Navarro, D. G., Caselli, P. et al. 2019, *A&A*, 624, A105
- Fuente, A., Rivière-Marichalar, P., Beitia-Antero, L. et al. 2023, *A&A*, 670, L13
- Fuentetaja, R., Agúndez, M., Cabezas, C., et al. 2022, *A&A*, 667, L4
- Gordon, V.D., McCarthy, M.C., Apponi, A.J. & Thaddeus, P. 2002, *ApJS*, 138, 297
- Hirahara, Y., Ohshima, Y. & Endo Y. 1994, *J. Chem. Phys.*, 101, 7342
- Kaifu, N., Suzuki, H., Ohishi, M., et al. 1987, *ApJ*, 317, L111
- Laas, J. C., & Caselli, P. 2019, *A&A*, 624, A108
- Marcelino, N., Puzzarini, C., Agúndez, M. et al. 2023, *A&A*, 674, L13
- McCarthy, M.C., Vrtilek, J.M., Gottlieb, E.W. et al. 1994, *ApJ*, 431, L127
- McCarthy, M.C., Cooksy, A.L., Mohamed, A. et al. 2003, *ApJS*, 144, 287
- McElroy, D., Walsh, C., Markwick, A. J., et al. 2013, *A&A*, 550, A36
- Millar, T. J., Walsh, C., Van de Sande, M., & Markwick, A. J. 2024, *A&A*, 682, A109
- Müller, H. S. P., Schlöder, F., Stutzki, J., Winnewisser, G. 2005, *J. Mol. Struct.*, 742, 215
- Nakajima, M., Sumiyoshi, Y. & Endo, Y. 2003, *J. Chem. Phys.*, 118, 7803
- Navarro-Almáida, D., Le Gal, R., Fuente, A. et al. 2020, *A&A*, 637, A39
- Pickett, H.M. 1991, *J. Mol. Spectrosc.*, 148, 371
- Pickett, H.M., Poynter, R. L., Cohen, E. A., et al. 1998, *J. Quant. Spectrosc. Radiat. Transfer*, 60, 883
- Saito, S., Kawaguchi, K., Yamamoto, S., et al. 1987, *ApJ*, 317, L115
- Tercero, F., López-Pérez, J. A., Gallego, J.D. et al. 2021, *A&A*, 645, A37
- Vastel, C., Quénard, D., Le Gal, R., et al. 2018, *MNRAS*, 478, 5514
- Vidal, T.H.G., Loison, J.-C., Jaziri, A.Y., et al. 2017, *MNRAS*, 469, 435
- Wakelam, V., Loison, J.-C., Herbst, E., et al. 2015, *ApJS*, 217, 20
- Yamamoto, S., Saito, S., Kawaguchi, K., et al. 1987, *ApJ*, 317, L119